THE JOURNAL OF PHYSICAL CHEMISTRY C

Article

pubs.acs.org/JPCC

# Anisotropic Shock Sensitivity of Cyclotrimethylene Trinitramine (RDX) from Compress-and-Shear Reactive Dynamics

Qi An,[†] Yi Liu,*[,†,‡] Sergey V. Zybin,[†] Hyungjun Kim,[§] and William A. Goddard, III*[,†,§]

[†]Materials and Process Simulation Center, 139-74, California Institute of Technology, Pasadena, California 91125, United States

[‡]School of Materials Science and Engineering, University of Shanghai for Science and Technology, Shanghai 200093, People's Republic of China

[§]Graduate School of Energy Environment Water Sustainability (EEWS), Korea Advanced Institute of Science and Technology (KAIST), Daejeon, 305-701, Republic of Korea

Supporting Information

**ABSTRACT:** We applied the compress-and-shear reactive dynamics (CS-RD) simulation model to study the anisotropic shock sensitivity of cyclotrimethylene trinitramine (RDX) crystals. We predict that, for mechanical shocks between 3 and 7 GPa, RDX is most sensitive to shocks perpendicular to the (100) and (210) planes, whereas it is insensitive for shocks perpendicular to the (120), (111), and (110) planes. These results are all consistent with available experimental information, further validating the CS-RD model for distinguishing between sensitive and insensitive shock directions. We find that, for sensitive directions, the shock impact triggers a slip system that leads to large shear stresses arising from steric hindrance, causing increased energy inputs that increase the temperature, leading to dramatically increased chemical reactions. Thus, our simulations demonstrate that the molecular origin of anisotropic shock sensitivity results from steric hindrance toward shearing of adjacent slip planes during shear deformation. Thus, strain energy density, temperature rise, and molecule decomposition are effective measures to distinguish anisotropic sensitivities. We should emphasize that CS-RD has been developed as a tool to distinguish rapidly (within a few picoseconds) between sensitive and insensitive shock directions of energetic materials. If the high stresses and rates used here continued much longer and for larger systems, it would ultimately result in detonation for all directions, but we have not demonstrated this.

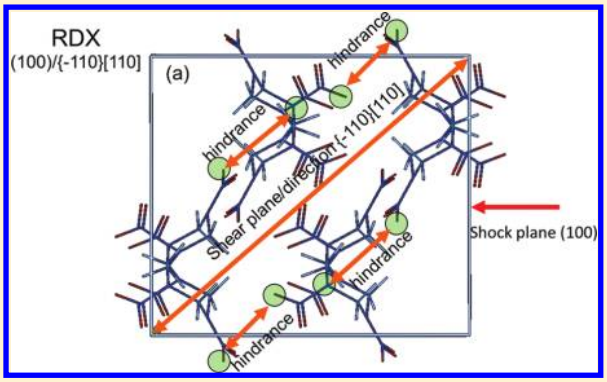


## I. INTRODUCTION

Energetic materials (EMs) are critical to applications ranging from civil constructions and military armaments to propulsion systems important in the aerospace and outer space industries. Empirical strategies for developing new energetic materials with high energy density have led to dramatic improvements. However, there is little understanding about the origin of the detonation sensitivity of energetic materials so crucial to safe storage and transport. Real energetic materials are heterogeneous with many interfaces, impurities, and defects, making it difficult to extract information about specific causes of sensitivity.

A breakthrough in understanding sensitivity was the experimental demonstration by Dick[1−3] that a large single crystal of pentaerythritol tetranitrate (PETN) displays dramatically different sensitivity to shocks in different directions, allowing one to ignore many complicating issues involving interfaces, impurities, and defects. For example, for PETN, the pressure threshold of detonation perpendicular to the (100) shock plane is at least ∼4 times that of the (110) shock plane.[4] In a previous report, we developed the compress-and-shear reactive dynamics (CS-RD) strategy to examine the anisotropic shock sensitivity of PETN[5] using the ReaxFF reactive force field.[6] Our simulations showed dramatically different sensitivities for various shock directions that agreed completely with available experimental observations. Another study for HMX[7] also showed excellent agreement between the predicted sensitive shock directions and available experimental observations on sensitivity.

The anisotropic detonation sensitivity of single crystals has been rationalized by various hypotheses, such as steric hindrance[1] and the formation of dislocation pile-up released by plasticity.[8,9] There are some indentation experiments[10−16] and direct shock experiments[17,18] on RDX crystals that suggest the possible slip systems for various shock directions. However, there is little direct experimental evidence on anisotropic detonation sensitivity because it is hard to synthesize large single crystals and measure anisotropic detonations required in such experiments.

**Received:** January 20, 2012
**Revised:** April 16, 2012
**Published:** April 17, 2012

Table 1. Results from CS-RD Simulations on the 22 Slip Systems Selected for the Five Shock Directions Based on 10% Compression Shear[a]

| sensitivity | shock plane | slip system | $T$ (K) at 8 ps | $NO_2$/RDX (%) at 10 ps | $\tau_{max} - \tau_c$ (GPa) | $(\tau_{max} - \tau_0)/\tau_0$ | $W$ (GPa) |
|---|---|---|---|---|---|---|---|
| **sensitive** | **(210)** | ***{120}<$\bar{2}$10>** | **1177** | **3.67** | **0.55** | **0.9** | **1.26** |
| | | {0$\bar{2}$1}<100> | 1107 | 1.85 | 0.44 | 3.0 | 1.12 |
| | | {021}<100> | 1096 | 1.80 | 0.44 | 3.2 | 1.12 |
| | | {010}<100> | 1101 | 2.63 | 0.43 | 4.2 | 1.07 |
| | | {0$\bar{1}$1}<100> | 1132 | 2.80 | 0.37 | 5.0 | 1.16 |
| | | {011}<100> | 1128 | 1.82 | 0.37 | 5.0 | 1.15 |
| **sensitive** | **(100)** | ***{$\bar{1}$10}<110>** | **1165** | **2.81** | **0.69** | **1.0** | **1.25** |
| | | {110}<1$\bar{1}$0> | 1173 | 3.76 | 0.60 | 1.2 | 1.25 |
| **insensitive** | **(111)** | ***{021}<100>** | **1098** | **1.90** | **0.47** | **3.3** | **1.15** |
| | | {010}<100> | 1071 | 1.19 | 0.35 | 4.4 | 1.06 |
| | | {011}<100> | 1143 | 2.78 | 0.58 | 5.6 | 1.14 |
| | | {010}<001> | 1163 | 3.38 | 1.17 | 5.6 | 1.27 |
| | | {0$\bar{2}$1}<100> | 1064 | 1.55 | 0.42 | 5.9 | 1.03 |
| | | {001}<010> | 985 | 0.05 | 0.16 | 10.7 | 0.93 |
| | | {0$\bar{1}$1}<100> | 1115 | 2.41 | 0.47 | 14.5 | 1.15 |
| **insensitive** | **(120)** | ***{010}<100>** | **1094** | **1.44** | **0.31** | **2.1** | **1.08** |
| | | {0$\bar{2}$1}<100> | 1117 | 2.34 | 0.40 | 2.6 | 1.13 |
| | | {$\bar{1}$20}<210> | 1200 | 4.84 | 0.92 | 2.9 | 1.36 |
| | | {0$\bar{1}$1}<100> | 1140 | 2.28 | 0.47 | 3.1 | 1.19 |
| **insensitive** | **(110)** | ***{010}<100>** | **1093** | **1.63** | **0.42** | **1.4** | **1.15** |
| | | {021}<100> | 1102 | 2.27 | 0.41 | 2.1 | 1.12 |
| | | {011}<100> | 1134 | 2.60 | 0.45 | 3.5 | 1.17 |

[a]The shear stress barrier over initial shear stress $(\tau_{max} - \tau_0)/\tau_0$ represents the shear driving force required to initiate shear along a slip system. We used this relative stress barrier to predict the slip system expected to prevail for each shock direction, which is marked by an asterisk, ∗. The strain energy density ($W$) is the imposed mechanical work required to initiate shear deformation over 4 ps. This strain energy density indicates the extra work needed to overcome the stress barrier and correlates directly with sensitivity. Also shown are the temperatures at 8 ps, the reaction product ratio, $NO_2$/RDX at 10 ps, and the stress overshoot.

In this paper, we use CS-RD to investigate the mechanism of sensitivity for a cyclotrimethylene trinitramine (RDX) single crystal for various shock directions using the original ReaxFF[6] reactive force field. This involves uniaxial compression in the shock direction, followed by shear deformation along possible shear planes. The CS-RD computational protocol was developed to capture the essential features of how shock processes relate to sensitivity while remaining sufficiently simple so that we can consider many different shock directions and shear planes at modest computational cost.

## II. SIMULATION METHODS AND PROCEDURES

**A. Simulation Models.** Three phases of RDX, $\alpha$, $\beta$, and $\gamma$,[19−23] have been identified experimentally. The most stable phase at ambient conditions is the $\alpha$ phase with orthorhombic symmetry (space group *Pbca*). The $\alpha$ phase transforms to the $\gamma$ phase at ∼4.5 GPa and 300 K, as detected by Raman spectroscopy.[22,23] The $\beta$ phase is formed either by evaporation of boiling solvent containing RDX,[24] by deposition of RDX from solution on a glass substrate,[25] or under high temperature above 470 K and high pressure above 3.6 GPa.[23]

Our simulations here focus on the most stable $\alpha$ phase. Starting from a unit cell of the $\alpha$ RDX crystal consisting of eight molecules with experimental lattice parameters,[19] we relaxed the structure with 1 ps of NPT molecular dynamics (0.1 fs time step) at 10 K and 0 GPa. This leads to lattice parameters of $a$ = 13.392 Å, $b$ = 11.828 Å, and $c$ = 11.238 Å, compared with experimental values at 300 K of $a$ = 13.182 Å, $b$ = 11.574 Å, and $c$ = 10.709 Å.

We then compressed the RDX crystal uniaxially by 10% (and 20%) for various shock directions. This precompression leads to initial hydrostatic stresses of ∼3.0 GPa (and 7.0 GPa). Previous shock experiments on RDX[17,18] measured the pressure over the range of $P$ < 2.25 GPa and for 7−20 GPa. Considering the temperature increase and plastic deformation in real shock experiments, we consider that our simulations using 10% and 20% compression can be compared to the available experiments.

We considered shocks perpendicular to five low index planes: (100), (210), (111), (110), and (120). For the sake of computational convenience, we rotated the compressed unit cell for each case so that the $x$−$z$ plane is the slip plane and $x$ is the slip direction in a Cartesian coordinate system. We then expanded the unit cell to a 10 × 10 × 2 supercell (1600 molecules or 33 600 atoms) or a 8 × 8 × 3 supercell (1536 molecules or 32 256 atoms) that we used in nonequilibrium reactive dynamics simulations at a constant shear rate.

**B. Selection of Slip Planes and Directions from the Resolved Shear Stress.** After compressing the 2 × 2 × 2 supercell of the RDX crystal, we minimized the structure using steepest descents for 5000 steps. Here, the energy difference converged to $<10^{-9}$ kcal/mol after 1000 steps. We then performed molecular dynamics minimization (NVT at 10 K) for 1 ps. After minimization, we averaged the full stress tensors over the structures obtained from the last 500 steps. We then projected this stress tensor onto various slip systems, defined by a combination of slip planes and slip directions, to obtain the resolved shear stresses (RSS) for each slip system. Since RSS reflects the driving force for shear deformation, we expect that the slip systems with larger RSS are more likely to be activated. We also expect that the angles between the slip plane/direction and the shock plane/direction should be close to 45° for the


dx.doi.org/10.1021/jp300711m | J. Phys. Chem. C 2012, 116, 10198−10206

Table 2. Results from CS-RD Simulations on the 24 Slip Systems Selected for the Five Shock Directions Based on 20% Compression Shear[a]

| sensitivity | shock plane | slip system | $T$ (K) at 5 ps | $NO_2$/RDX (%) at 8 ps | $\tau_{max} - \tau_c$ (GPa) | $(\tau_{max} - \tau_0)/\tau_0$ | $W$ (GPa) |
|---|---|---|---|---|---|---|---|
| **sensitive** | **(100)** | ***{110}<1$\bar{1}$0>** | **1199** | **21.2** | **1.61** | **0.7** | **1.67** |
| | | {$\bar{1}$10}<110> | 1185 | 17.2 | 1.51 | 0.8 | 1.65 |
| | | {101}<10$\bar{1}$> | 1095 | 11.8 | 0.47 | 2.6 | 1.49 |
| | | {$\bar{1}$01}<101> | 1109 | 13.4 | 0.43 | 2.6 | 1.50 |
| **sensitive** | **(210)** | ***{120}<$\bar{2}$10>** | **1131** | **11.7** | **0.85** | **1.9** | **1.62** |
| | | {021}<100> | 1017 | 5.6 | 0.45 | 2.3 | 1.33 |
| | | {010}<100> | 992 | 5.0 | 0.72 | 2.4 | 1.27 |
| | | {0$\bar{2}$1}<100> | 1039 | 7.5 | 0.40 | 2.7 | 1.33 |
| | | {011}<100> | 1054 | 9.3 | 0.50 | 2.9 | 1.38 |
| | | {0$\bar{1}$1}<100> | 1054 | 8.9 | 0.53 | 4.3 | 1.41 |
| **insensitive** | **(111)** | ***{021}<100>** | **1045** | **8.1** | **0.65** | **2.6** | **1.42** |
| | | {010}<001> | 1056 | 8.1 | 0.94 | 2.9 | 1.44 |
| | | {001}<010> | 986 | 5.1 | 0.36 | 3.5 | 1.31 |
| | | {0$\bar{2}$1}<100> | 971 | 3.9 | 0.36 | 3.8 | 1.23 |
| | | {011}<100> | 1128 | 14.3 | 0.73 | 4.8 | 1.43 |
| | | {010}<100> | 957 | 4.5 | 0.27 | 8.7 | 1.27 |
| **insensitive** | **(120)** | ***{010}<100>** | **1018** | **5.3** | **0.94** | **1.9** | **1.37** |
| | | {$\bar{1}$20}<210> | 1167 | 17.2 | 1.81 | 2.0 | 1.77 |
| | | {021}<100> | 1052 | 9.1 | 1.10 | 2.5 | 1.47 |
| | | {011}<100> | 1092 | 10.4 | 1.19 | 3.1 | 1.56 |
| **insensitive** | **(110)** | ***{010}<100>** | **979** | **5.1** | **0.38** | **1.2** | **1.24** |
| | | {101}<10$\bar{1}$> | 1139 | 17.4 | 0.75 | 1.2 | 1.61 |
| | | {021}<100> | 1041 | 7.4 | 0.82 | 1.3 | 1.39 |
| | | {011}<100> | 1091 | 10.4 | 0.78 | 1.9 | 1.50 |

[a]The shear stress barrier over the initial shear stress $(\tau_{max} - \tau_0)/\tau_0$ represents the shear driving force required to initiate shear along a slip system. We use this relative stress barrier to predict the slip system expected to prevail for each shock direction, which is marked by an asterisk, ∗. The strain energy density ($W$) is the imposed mechanical work required to initiate shear deformation over 3 ps. This strain energy density indicates the extra work needed to overcome the stress barrier and correlates directly with sensitivity. Also shown are the temperatures at 5 ps, and the reaction product ratio, $NO_2$/RDX at 8 ps, and the shear stress overshoot.

preferred slip system. On the basis of these criteria, we considered the largest RSS of the slip systems with angles in the range of 30−60°. In addition, we considered all slip systems suggested from previous experiments.[17−23] This led to 22 possible slip systems for 10% precompression and 24 slip systems for 20% precompression for the five shock directions on which we performed CS-RD simulations.

**C. Compressive Shear Reactive Dynamics (CS-RD).** To obtain a mechanistic understanding of anisotropic shock sensitivity, we developed the CS-RD model that first compresses uniformly along the shock direction and then shears at a uniform rate along the most plausible slip systems. We found for PETN and HMX that the CS-RD model captures the essential character related to sensitivity of real shock processes (mechanical shock, activated slip systems).[5,7]

The CS-RD was developed as a tool to quickly distinguish between sensitive and insensitive shock directions. The time scales are far too short and the shear rates are far too large for a realistic simulation of shock decomposition. For example, we carry out full ReaxFF reactive dynamics simulations on shock processes[26] and considered a periodic cell with 3.7 million atoms to describe PBX (RDX with polymer binder). This study extracted information about the origin of hot spot formation. We found that the hot spot arises from shear stresses induced by differential relaxation of the shocked material at an asperity. Such calculations required huge computer clusters for very long times. In contrast, the CS-RD model is much simpler, requiring only thousands of atoms and is practical on a single central processing unit (CPU).

Starting with the compressed and minimized cells described above, we heated the systems slowly (from 10 to 300 K over 1.0 ps) to ensure that no chemical bonds were broken during heating. We then equilibrated the system with NVT for 1 ps at 300 K. We then expanded the unit cell to a large supercell (10 × 10 × 2 or 8 × 8 × 3) for each of the selected slip systems under the five shock directions (Tables 1 and 2). Finally, we carried out shear deformation reactive dynamics (RD) on the compressed and rotated supercells for up to 10 ps by deforming the supercells every 10 time steps (1.0 fs) at a constant shear rate 0.5/ps. In this deformation we convert the *xyz* coordinates of each atom to scaled coordinates (converting to the nonorthogonal unit cell coordinate system and normalizing with the supercell parameters *a*, *b*, *c*), apply the shear (changing the cell angle), and then transform back to obtain the new *xyz*. This leads to very small distortions of the bond lengths and angles, which then relax over the next 10 steps of dynamics. No temperature constraint was applied during the constant shear rate RD.

**D. Steric Hindrance Contour Maps.** A schematic illustration of the molecule contacts during shear deformation is shown in Figure 1. To examine the correlation between sensitivity and steric hindrance, we propose a geometry-based method to visualize and measure the extent of steric hindrance. First, we compressed the molecular crystal by scaling the center of mass for each molecule along a given shock direction. We then projected the full geometry of the undistorted molecules onto a plane perpendicular to both the shear plane and the shear direction. We define a scoring scheme for molecule

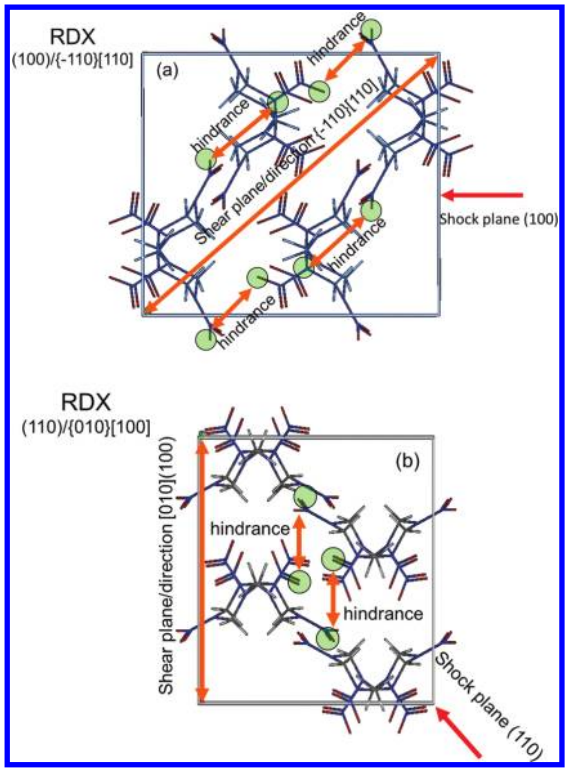


**Figure 1.** Unit cells of the RDX crystal including schematic illustrations of molecule contacts during shear deformation: (a) sensitive shock plane (100) with slip system $\{\bar{1}10\}/<110>$ with large steric hindrance; (b) insensitive shock plane (110) with slip system $\{010\}/<100>$ with small steric hindrance.

overlaps based on the covalent bond radius for each atom as follows: If molecules on adjacent planes overlap after projection, one point is given to the position on the project plane. On the basis of the overlap scores, we plot a 2-D *steric hindrance contour map*, where the overlapped regions indicate the areas where steric hindrance may occur during the shear process. The areas of the overlapped regions are summed, followed by normalization by the area of the projected cross section. The ratio of overlapped regions relative to the projected cross section provides a quantitative measure of the extent of steric hindrance, hereafter denoted as the *steric hindrance index* (SHI). This SHI analysis method is efficient and independent of force fields since it only requires crystal structures as input without the need of expensive dynamic simulations. On the other hand, since the SHI analysis is based on the rigid molecule geometry, it does not take into account geometry relaxation and chemical reactions.

**E. Bond Fragment Analysis.** To analyze the numerous reactions that occur during ReaxFF simulations, we need a systematic criterion to identify molecular fragments. To enable the automatic and systematic analysis of chemical reactions from ReaxFF simulation trajectories, we developed a molecular fragment analysis program, BondFrag. A general criterion often used to determine atomic connectivity involves a comparison of interatomic distances with the van der Waals (vdW) radii. However, the vdW radii defined under ambient conditions are not appropriate for highly compressed and detonative conditions. Instead, to provide a quantitative criterion for defining the presence of chemical bonds, we use the bond order values defined in ReaxFF, which range is from 0 to 1 for the systems considered here. We optimized the bond order cutoff values from simulations of several energetic materials systems. These cutoff values are tabulated in Table S1 in the Supporting Information for various atom pairs.

To distinguish instantaneous fluctuations that might decrease the BO below our cutoff, but which does not actually break (or form) a bond, we excluded from our fragment analysis any newly created (or annihilated) bonds that were annihilated (or created) within the time window of 1 ps.

After determining the molecular fragments based on bond order cutoff values with the 1 ps time window, BondFrag assigns a unique identification number to each molecular fragment to trace the reaction pathways and calculate such molecular properties as a center of mass, dipole moment, and molecular charge.

## III. RESULTS AND DISCUSSION

**A. Resolved Shear Stress.** We calculated the stress tensors of the minimized and compressed crystals for the five shock planes under consideration. We then projected the stress tensor onto all the low index slip systems ranging from $\{\bar{2}\bar{2}\bar{2}\}$ to $\{222\}$ to obtain the RSS of each slip system for each shock plane. Tables S2−S11 in the Supporting Information list the RSS results of some selected slip systems for five shock planes under two precompressions, together with the angles between the shock plane/slip plane ($\varphi$) and the shock direction/slip direction ($\psi$) for the possible slip systems.

Previous solution etch pitting experiments[11] on the RDX crystal suggested that (010) is the primary slip plane, which was confirmed by X-ray crystallography studies.[16] Microindentation experiments on the (120), (010), (111), and $(\bar{2}10)$ planes indicated that $\{021\}/<100>$ is an alternative primary slip system.[12−15] Recent nanoindentation experiments also suggested that $\{011\}/<100>$ is a slip system.[10,12,15] In addition, $\{021\}/\pm<01\bar{2}>$ were suggested as possible slip systems based on geometric considerations of intermolecular displacement.[12−16]

We chose six possible slip systems for the (210) shock: $\{120\}<\bar{2}10>$, $\{021\}<100>$, $\{0\bar{2}1\}<100>$, $\{010\}<100>$, $\{011\}<100>$, and $\{01\bar{1}\}<100>$. The $\{120\}<\bar{2}10>$ slip system has the largest RSS with the angle in the range of 30−60°, while the other five slip systems were proposed in a previous study.[18]

For the (111) shock, we chose the five slip systems proposed for the (210) shock above, $\{010\}<001>$, as suggested by Dang,[18] and $\{001\}<100>$, as suggested by previous nonreactive force field MD simulation.[27]

No slip systems were suggested experimentally for (100) shocks, so we chose the slip systems with the largest RSS and appropriate angles between 30 and 60°.

For the shock planes (120) and (110), we chose the slip systems with the largest RSS and angles in the range of 30−60° or those that were suggested in previous nanoindentation experiments.[19−23]

All together, we chose 22 slip systems for the five shock planes: two slip systems for the (100) shock, six for the (210) shock, seven for the (111) shock, four for the (120) shock, and three for the (110) shock, respectively, as listed in Table 1.

**B. Compressive Shear Reactive Dynamics.** *1. Results.* The hint that shear deformation is critical to understanding the sensitivity of energetic materials was provided by Plazkins's experiments showing initiation of detonation along directions corresponding to the maximum shear stress.[28] The CS-RD model was developed to understand which aspects of the shock process are related to sensitivity by first compressing the


dx.doi.org/10.1021/jp300711m | J. Phys. Chem. C 2012, 116, 10198−10206

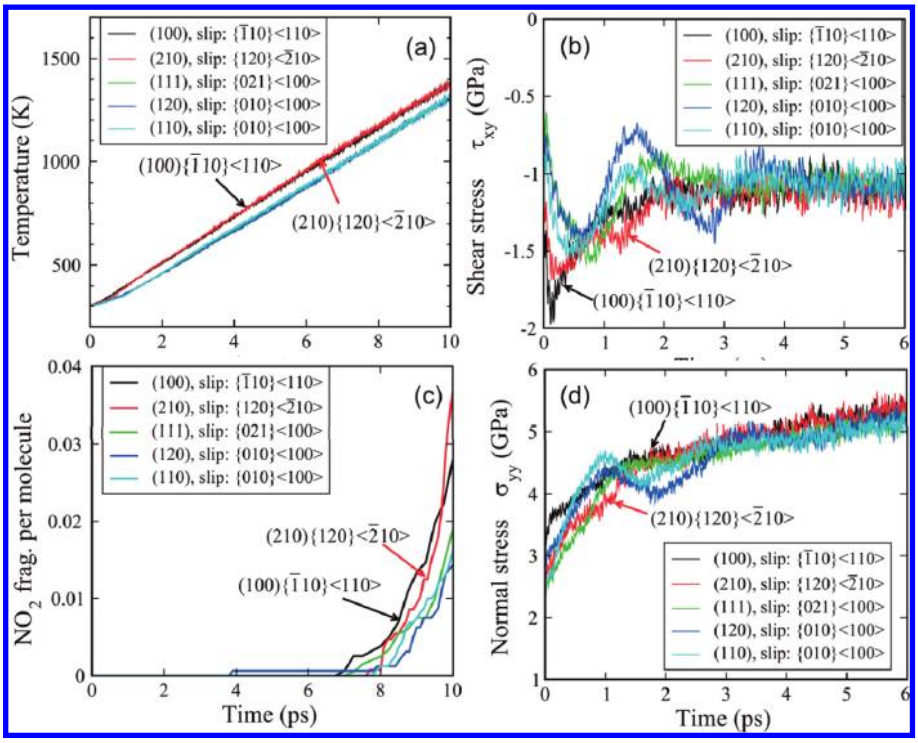


**Figure 2.** CS-RD results for the preferred slip system predicted for each of the five shock directions (after 10% precompression): (a) temperature, (b) shear stress, (c) $NO_2$ products, and (d) normal stress as a function of time under the five shock directions in shear simulation. These calculations identify the (210)/{120}<$\bar{2}$10> and (100)/{$\bar{1}$10}<110> shock/slip systems as the two most sensitive cases. In both cases, the large shear stress overshoot in (b) for 0−0.5 ps results from an initial bad steric overlap. This bad steric contact is manifested in the large normal stress observed for 0−0.5 ps in (d). The external mechanical work necessary to overcome the large stress barrier (see Figure 3c) induces the larger temperature increase by 1 ps compared with the other slip systems, as shown in (a). This extra temperature remains for the rest of the simulation, leading to significantly more molecule decomposition starting at 7 ps, as shown in (c).

crystals (by 10% and 20%), followed by shear deformation along various slip systems. For the selected slip systems, we compressed the crystals and equilibrated for 1 ps NVT MD at $T$ = 300 K. This leads to calculated total pressures of 2.6−3.2 GPa after 10% compression and 7.0−7.6 GPa after 20% compression. We focus our discussions on the shear simulations from the 10% compression since the $\alpha$ phase is the most stable phase under the pressure of 2.6−3.2 GPa. We also present the results of 20% compression-shear simulations that can be compared to the multiple shock experiments leading to decomposition.[18] The results of 10% and 20% compression are compared to examine the effects of compression ratio.

Table 1 (10% precompression) tabulates the results from shear simulations for the 22 selected slip systems, whereas Table 2 (20% precompression) does the same for the 24 slip systems. For each of the five shock planes, we selected the most probable slip system, with the results summarized in Figure 2 (10% precompression) and Figure 5 (20% precompression). These results from the early stage of the shear process are expected to be important in understanding the anisotropic sensitivity under mechanical shock compression.

The criterion to select the most probable slip systems is the shear stress barrier with respect to the initial shear stress, $(\tau_{max} - \tau_0)/\tau_0$. This relative stress barrier correlates with the initial driving force required to activate a slip system. We expect that the slip system with a minimum relative stress barrier is more likely to be activated. It is possible that a particular shock could trigger multiple slip systems, but we choose only the most probable slip system for further comparisons of sensitivities among various shock directions. On the basis of the relative shear stress barrier, we chose the five most probable slip systems corresponding to the five shock directions: {$\bar{1}$10}/<110> for the (100) shock, {120}/<$\bar{2}$10> for the (210) shock, {021}/<100> for the (111) shock, {010}/<100> for the (120) shock, and {010}/<100> for the (110) shock under 10% precompression.

Shear deformation introduces mechanical work into the systems, which we calculate from the total integrated energy to induce shearing until the shear stress is a constant for all directions. This imposed mechanical work can be quantified in terms of the strain energy density obtained by integrating the shear stress along the stress−strain curve to a point before the mechanical work starts converting to thermal and chemical energies. Since the shear rate in our simulation is constant (0.5/ps), the integration can be carried out using the stress−time curve (Figures 2b and 5b) and converting the time to the shear strain. We did the integration to 4 ps for 10% precompression and to 3 ps for 20% precompression when the shear stresses converged to constant values for all five shock directions.

For 10% precompression, the (100) and (210) shocks led to a strain energy density of 1.25 and 1.26 GPa, respectively. The (111), (120), and (110) shocks led to smaller strain energy densities: 1.15, 1.08, and 1.15 GPa, respectively. The large strain energy density for (100) and (210) shocks correlates with their large sensitivity because it indicates that more mechanical work is available to convert to thermal or chemical energies, leading to higher temperatures and more chemical decompositions. For sensitive directions, more mechanical work is required during the shearing process. After molecules


dx.doi.org/10.1021/jp300711m | J. Phys. Chem. C 2012, 116, 10198−10206

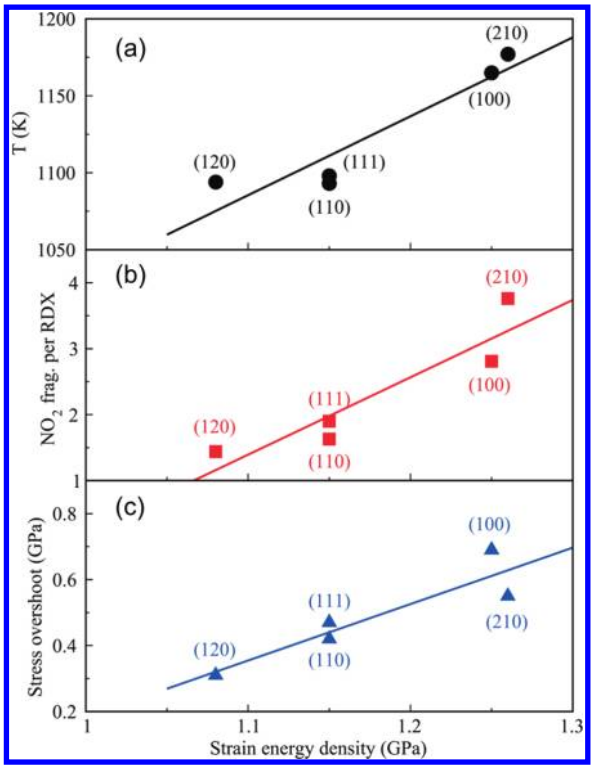


**Figure 3.** Correlations between strain energy density (integration of shear stress up to 4.0 ps in Figure 2b) and other sensitivity measurements for 10% precompression: (a) temperature at 8 ps, (b) $NO_2$ production at 10 ps, and (c) stress overshoot during CS-RD. The large strain energy density for the (210) and (100) shock planes leads to the large temperature increase, the increased $NO_2$ dissociation, and the large stress overshoot during CS-RD. This makes these the sensitive shock directions and indicates that strain energy density is the determining factor for sensitivity.

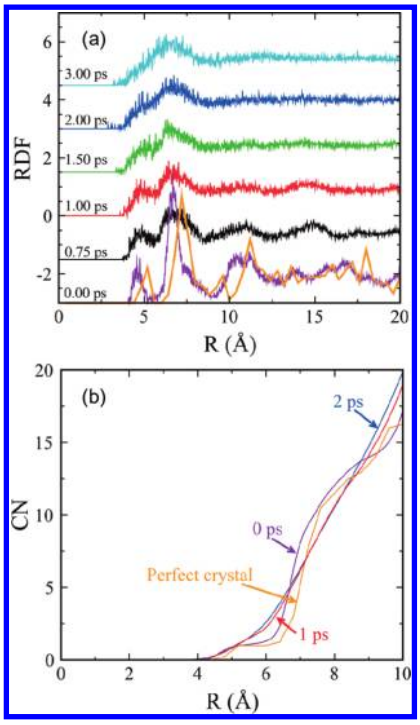


**Figure 4.** Structural analysis for the sensitive (100) shock and {$\bar{1}$10}/<110> slip system (10% precompression). The radial distribution function (RDF) for the center of mass of each RDX molecule is shown in (a), indicating that the crystalline character is retained up to ~1 ps, and the integrated coordination numbers (CN) in (b) remain that of the experimental structure at room temperature (the orange line). Compared with the perfect crystal, the RDF at 0 ps in (a) is shifted to the left due to the 10% precompression. By 2 ps, the system has the amorphous structural characteristics of the liquid phase of RDX condensed systems.

overcome the first large barriers (before 4 ps), the shear stress decreases, indicating that some imposed mechanical work converts to heat continuously being used to break chemical bonds starting at ~6.5 ps.

Figure 2 shows the evolution of temperature, $NO_2$ production, shear stress, and normal stress ($\sigma_{yy}$) during the 10 ps of shear simulations for 10% precompression. We found that the temperature increased most significantly, from 300 to 1165 K after 8 ps for the (100) shock and the {$\bar{1}$10}/<110> slip system, and to 1177 K for the (210) shock and the {120}/<$\bar{2}$10> slip system. The temperatures increased moderately to 1098 K for the (111) shock and {021}/<100> slip system, to 1094 K for the (120) shock and {010}/<100> slip ystem, and to 1093 K for the (110) shock and {010}/<100> slip system. The temperature increases also indicate that (100) and (210) are the most sensitive shock directions, whereas (120), (110), and (111) are insensitive shock directions.

To track the chemical processes during the CS-RD process, we analyze the molecular fragments from the corresponding ReaxFF MD trajectories based on a bond order cutoff criterion. The sensitivity prediction based on the strain energy density discussed above is further supported by the fragment analysis for $NO_2$, the product of the initial dissociation of RDX under shock compression. Figure 2c shows that the most sensitive (100) and (210) shocks led to 2.81% and 3.67% $NO_2$ per RDX molecule at 10 ps, respectively. On the other hand, the less sensitive (111), (120), and (110) shocks led to 1.90, 1.44, and 1.63% $NO_2$/RDX, respectively. We found that the $NO_2$ production occurs mainly after 6.5 ps when the temperature increases above 1000 K.

The overshooting of the shear stress, defined as $\tau_{max} - \tau_c$, is correlated to the imposed mechanical work during shear. The most sensitive (100) and (210) shocks led to a shear stress overshoot of 0.69 and 0.55 GPa, respectively, the largest ones among all shock directions. The less sensitive (111), (120), and (110) shocks led to stress overshoots of 0.47, 0.31, and 0.42 GPa, respectively.

The shear stress barrier measures the energy barrier of shear deformation. As Figure 2b shows, the shear stresses maximize within the first picoseconds. For the most sensitive (100) shock, the shear stress maximizes at ~0.2 ps and then relaxes to a constant value. On the other hand, for the less sensitive (120) shocks, the shear stress oscillates before relaxing to constant values. This indicates that the shear deformation encounters several small energy barriers in these slip systems. The normal stress shown in Figure 2d also indicates the dramatic difference for various slip systems.

Figure 3 (10% precompression) and Figure 6 (20% precompression) show good correlations between strain energy density and temperature, $NO_2$ population, and stress overshoot. Results of all the CS-RD simulations summarized in Figure S-1 in the Supporting Information show clearly a linear relationship between the strain energy density and temperature, $NO_2$ production, and stress overshoot. The imposed mechanical work is the origin of the temperature increase and $NO_2$


dx.doi.org/10.1021/jp300711m | J. Phys. Chem. C 2012, 116, 10198−10206

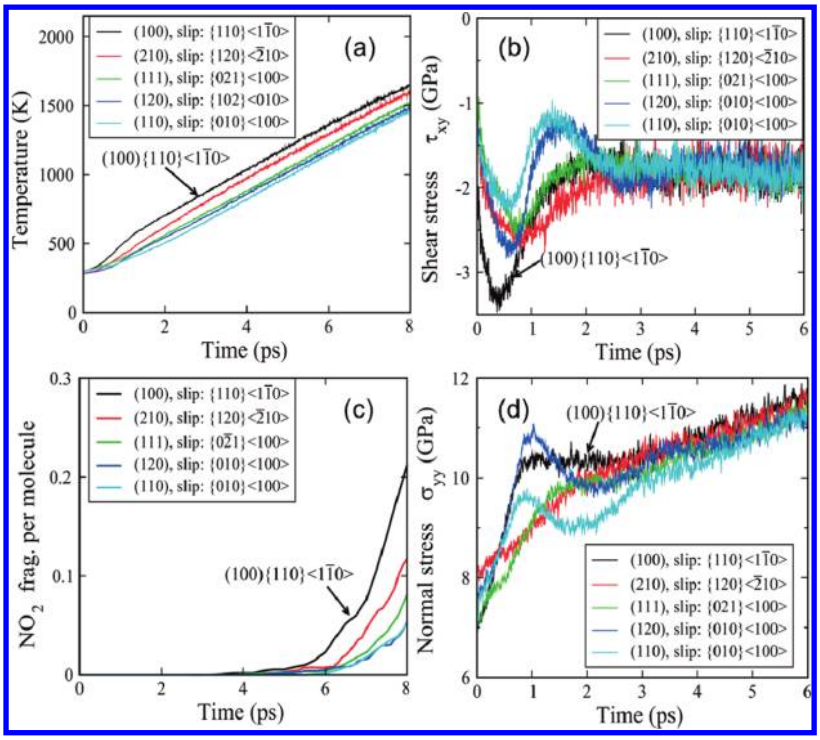


**Figure 5.** CS-RD results for the preferred slip system predicted for each of the five shock directions (after 20% precompression): (a) temperature, (b) shear stress, (c) $NO_2$ products, and (d) normal stress as a function of time under various shock directions in shear simulation. These calculations identify that the (210)/{120}<$\bar{2}$10> and the (100)/{110}<1$\bar{1}$0> shock/slip systems are the two most sensitive cases. In both cases, the large shear stress overshoot in (b) for 0−0.5 ps results from an initial bad steric overlap. This bad steric contact causes the large normal stress observed between 0 and 0.5 ps in (d). The external mechanical work necessary to overcome the large stress barrier leads to the large extra temperature increase by 1 ps compared with the other slip systems shown in (a). This extra temperature remains for the rest of the simulation, leading to significantly more molecule decomposition starting at 4 ps, as shown in (c).

production for various shock directions. Since shear stresses converge to similar values when the system becomes amorphous, the strain energy density integrated at an early stage represents mostly the characteristics of the energy landscape specific to a given shock and slip system. Thus, the strain energy density can be used as a useful criterion to distinguish the anisotropic sensitivities among various shock directions. After overcoming the initial stress barriers, the temperature rise and molecule decomposition become major measurements for sensitivity since the thermal energy and chemical energy, together with residual strain energy, came from the imposed mechanical work.

The process of shear deformation is described as follows. First, molecules on adjacent slip planes are pushed into each other as they shear along a given slip direction, indicated by the increased shear stress. After passing through the first energy barrier (<1 ps), there are few additional barriers to overcome. After about 3 ps, the system becomes amorphous, as indicated by radial distribution functions (RDFs) and coordination numbers (CNs) shown in Figure 4 for the (100) shock and {$\bar{1}$10}/<100> slip system. The work done to overcome molecular interactions increases the temperature until it is high enough to break the N−N bonds to form $NO_2$ products.

After the system becomes amorphous, the shear stresses reach constant values, leading to the viscosity

$$\tau_{xy} = \eta\gamma_{xy} \quad (1)$$

Here, $\tau_{xy}$ is the converged shear stress (GPa) for the RDX amorphous, $\gamma_{xy}$ is the shear rate 0.5 $ps^{-1}$, and $\eta$ is viscosity in the unit of poise. We calculate a viscosity of 2.1 cP for 10% compression (5 GPa pressure after the shear stress converges) and 3.6 cP for 20% compression (11 GPa pressure after the shear stress converges).

For 20% precompression, we chose 24 slip systems for CS-RD simulations of the five shock directions (see tables SI7−SI11 in the Supporting Information for more details). Under 20% precompression, for all systems except the (100) shock, we selected the same slip systems based on the shear stress barrier over the initial shear stress as the possible activated slip systems for the five shock directions. On the basis of the strain energy density, shear stress overshoot, temperature rise, stress barrier, and $NO_2$ production, we found that (100) and (210) shocks are still the most sensitive, whereas (111), (120), and (110) are insensitive shock directions.

We also performed the CS-RD simulation on 30% precompression for (100), (110), and (111) shock planes. The CS-RD results are in Table S-12 in the Supporting Information. We found that (100) is still a sensitive shock plane, whereas (110) and (111) are insensitive shock planes. These results are consistent with 10% and 20% precompression.

*2. Discussion.* Our CS-RD results for 10% precompression and 20% precompression are consistent with the shock experiments,[18] suggesting that (100) and (210) are sensitive shock directions, whereas (111) is an insensitive shock direction at the pressures of 7−20 GPa.[18]

The slip system {120}/<$\bar{2}$10> for the (210) shock plane is not observed in the nanoindentation experiment,[19−23] but it is suggested as the possible slip system under high compression based on our CS-RD simulation. We believe that this slip


dx.doi.org/10.1021/jp300711m | J. Phys. Chem. C 2012, 116, 10198−10206

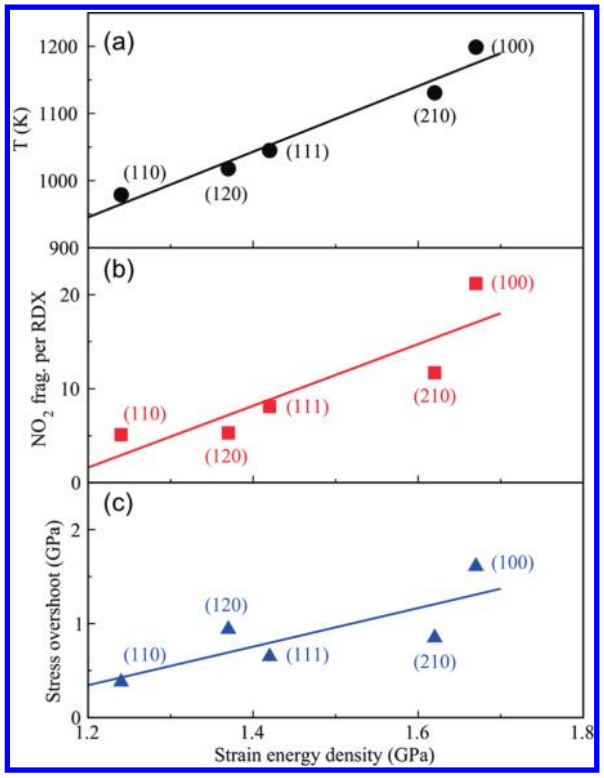


**Figure 6.** Correlations between the strain energy density (integration of shear stress up to 3.0 ps in the Figure 5b) and other sensitivity measurements for 20% precompression: (a) temperature at 5 ps, (b) $NO_2$ production at 8 ps, and (c) stress overshoot during CS-RD. The large strain energy density for the sensitive (100) shock plane and somewhat less for the (210) plane lead to the high temperature increase, more $NO_2$ production, and large stress overshoot during CS-RD.

system may not be easily activated under low pressure due to the multiple shear stress barriers shown in Figure 2b. The high

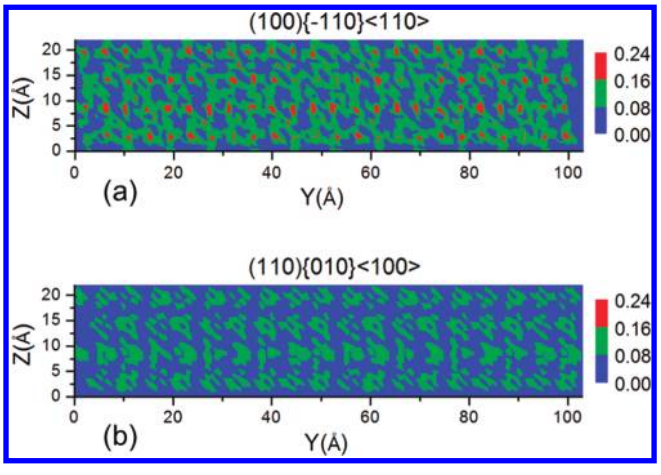


**Figure 7.** Steric hindrance counter maps projected along the $x$ slip direction for (a) the (100) shock with the $\{\bar{1}10\}/<110>$ slip system found to be the most sensitive, with a steric hindrance index (SHI) of 0.59, and (b) the (110) shock and {010}/<100> slip systems found to be the least sensitive, with an SHI of 0.43 after 10% precompression. The larger contact areas/scores and interconnected contact pattern for the (100) shock indicate larger molecular steric hindrance during shear deformation, which is responsible for its large sensitivity.

compression is necessary to increase the initial shear stress and activate this slip system.

To explain the shock experiment of the (111)-oriented RDX single crystal, Cawkwell et al[27] carried out nonreactive MD simulations on the shock wave propagation along the <111> direction in the RDX single crystal. They found that the partial dislocations 0.16{001}/<010> are nucleated homogeneously when the shock pressure is greater than ~1.3 GPa. These partial dislocations suppress the activation or movement of other dislocations. Thus, they proposed an anomalous plasticity hardening model to explain the abnormal elastic–plastic response in RDX (111) shock experiments. On the basis of their plasticity hardening model, they predict that an insensitive-to-sensitive transformation for the (111) shock occurs as the pressure increases from 1.25 to 2.0 GPa. Their study suggests that the relation of shock sensitivity and slip systems is extremely complex.

Our previous PBX shock simulation[26] showed that shock at the asperity of a nonuniform interface of heterogeneous materials leads to shear relaxation that causes shear stresses along the nonuniform interface. These shear stress relaxations result in energy dissipation at the interface that leads to a local significant increase in temperature. This increase in temperature leads to bond breaking in energetic materials, which leads eventually to detonation. This study indicates that shear slip plays essential roles in the shock sensitivity for the molecular crystal

Our CS-RD model examines each possible slip system separately, assuming that the dominant one is the slip system having the lowest value of the barrier to plastic deformation divided by the component of the stress along this direction. In some cases, we find more than one such slip system.

Our CS-RD model might not be appropriate for the situations in which complex interactions of various slip systems play important roles. For example, we find that the 0.16{001}/<010> partial dislocation will not be activated in the cases of (100), (110), (120), and (210) shocks since there is no resolved shear stress in the (001) plane. For the (111) shock, the CS-RD model would not capture the plastic hardening in Cawkwell's study.[27] Previous experiments[18] show that the (111) shock is less sensitive than (100) and (210) shocks when the pressure is greater than 7 GPa. This indicates that plastic hardening might disappear under very high pressure where chemistry might play an important role. Our CS-RD model gives consistent results as the high-pressure experiment that validates our model under a high-pressure environment.

**C. Steric Hindrance Analysis.** To understand the molecular origin of sensitivity, we now examine the relationship between sensitivity and steric hindrance estimated from the initial molecular geometry. Figure 7 shows the steric hindrance contour maps for the (100) shock and $\{\bar{1}10\}/<110>$ slip system, and the (110) shock and {010}/<100> slip system. The steric hindrance contour map represents the overlapped regions and possible contact areas during shear deformation. These maps indicate that the shear deformation induced by the (100) shock encounters more bad contacts than those for the (110) shock. For the (100) shock, the interconnected contact patterns indicate more intensive contacts and the higher overlap score represents more multiple contacts.

On the other hand, for the (110) shock, the gaps between contact regions provide more room for geometry relaxation when molecules conflict. Indeed, the SHI of the sensitive (100) shock is 0.59, indicating 16% more overlap regions than the


dx.doi.org/10.1021/jp300711m | J. Phys. Chem. C 2012, 116, 10198–10206

insensitive (110) shock with an SHI of 0.43. Our calculations also show that SHI increases with the compression ratio. This means that strong shocks with large compression cause more steric hindrance than weak shocks. This analysis of the steric hindrance contour map and SHI support the steric hindrance explanation for anisotropic sensitivity.

## IV. CONCLUSIONS

We find that the CS-RD protocol successfully predicts that (100) and (210) are the most sensitive shock directions for RDX, whereas (120), (111), and (110) shocks are insensitive. The predicted relative sensitivities are consistent with the previous RDX shock experiments at pressures around 7−20 GPa.

Now that the CS-RD protocol has been validated for PETN, HMX, and RDX, for which the experimental data are most complete, we can proceed to examine new energetic systems to predict which ones would be least sensitive. Also, we can consider heterogeneous systems, with defects and impurities, to determine the roles in determining sensitivity.

We should emphasize here that CS-RD is aimed toward a rapid assay of anisotropic sensitivity for use when considering new energetic materials. We deliberately impose rather severe conditions to create stresses comparable to experiments, but driven at high rates to examine sensitivity rapidly. The high shear rates used here already lead to a continuously shearing fluid system by 10 ps, and all slip systems considered here would rapidly detonate under these conditions. However, even so, we find dramatic differences between sensitive and insensitive slip systems, as reflected in strain energy density, temperature rise, and molecule decomposition.

Our reactive dynamics studies for PETN, HMX, and RDX support the concept that molecular steric hindrance contributes to the origin of anisotropic sensitivity of energetic materials. Molecular steric hindrance is thus critical to the development of energetic materials with reduced sensitivity.

## ■ ASSOCIATED CONTENT

### Supporting Information

The bond order cutoff table for bond fragment analyses, the resolved shear stress for 10% and 20% precompressions, the CS-RD simulation results of three shock directions for 30% precompression, and the correlation of strain energy density with other measurements of sensitivity for 10% precompression. This material is available free of charge via the Internet at http://pubs.acs.org.

## ■ AUTHOR INFORMATION

### Corresponding Author

*E-mail: wag@wag.caltech.edu.

### Notes

The authors declare no competing financial interest.

## ■ ACKNOWLEDGMENTS

This work was supported by the Office of Naval Research (N00014-05-1-0778 and N00014-09-1-0634; Cliff Bedford, program manager), the Army Research Office (W911NF-05-1-0345 and W911NF-08-1-0124; Ralph Anthenien, program manager), and Los Alamos National Laboratory (Ed Kober, program manager). Some computations in this work were carried out in the Arctic Region Supercomputer Center, DOD HPC system. We thank Dr. Betsy Rice and Larry Davis for assistance.

## ■ REFERENCES

(1) Dick, J. J. *Appl. Phys. Lett.* **1984**, *44*, 859−861.
(2) Dick, J. J.; Ritchie, J. P. *J. Appl. Phys.* **1994**, *76*, 2726−2737.
(3) Dick, J. J.; Mulford, R. N.; Spencer, W. J.; Pettit, D. R.; Garcia, E.; Shaw, D. C. *J. Appl. Phys.* **1991**, *70*, 3572−3587.
(4) Yoo, C. S.; Holmes, N. C.; Souers, P. C.; Wu, C. J.; Ree, F. H.; Dick, J. J. *J. Appl. Phys.* **2000**, *88*, 70−75.
(5) Zybin, S. V.; Goddard, W. A.; Xu, P.; van Duin, A. C. T.; Thompson, A. P. *Appl. Phys. Lett.* **2010**, *96*, 081918.
(6) van Duin, A. C. T.; Dasgupta, S.; Lorant, F.; Goddard, W. A. *J. Phys. Chem. A* **2001**, *105*, 9396−9409.
(7) Zhou, T.; Zybin, S. V.; Liu, Y.; Huang, F.; Goddard, W. A. *J. Appl. Phys.* **2012**, submitted forpublication.
(8) Armstrong, R. W. *Cent. Eur. J. Energ. Mater.* **2005**, *2*, 55−70.
(9) Walley, S. M.; Field, J. E.; Greenaway, M. W. *Mater. Sci. Technol.* **2006**, *22*, 402−413.
(10) Ramos, K. J.; Hooks, D. E.; Bahr, D. *Philos. Mag.* **2009**, *89*, 2381−2402.
(11) Connick, W.; May, F. G. J. *J. Cryst. Growth* **1969**, *5*, 65−69.
(12) Elban, W. L.; Hoffsommer, J. C.; Armstrong, R. W. *J. Mater. Sci.* **1984**, *19*, 552−566.
(13) Halfpenny, P. J.; Roberts, K. J.; Sherwood, J. N. *J. Mater. Sci.* **1984**, *19*, 1629−1637.
(14) Elban, W. L.; Armstrong, R. W.; Yoo, K. C.; Rosemeier, R. G.; Yee, R. Y. *J. Mater. Sci.* **1989**, *24*, 1273−1280.
(15) Gallagher, H. G.; Halfpenny, P. J.; Miller, J. C.; Sherwood, J. N. *Philos. Trans. R. Soc. London A* **1992**, *339*, 293−303.
(16) Mcdermott, I. T.; Phakey, P. P. *J. Appl. Crystallogr.* **1971**, *4*, 479−481.
(17) Hooks, D. E.; Ramos, K. J.; Martinez, A. R. *J. Appl. Phys.* **2006**, *100*, 024908.
(18) Dang, N. C.; Dreger, Z. A.; Gupta, Y. M.; Hooks, D. E. *J. Phys. Chem. A* **2010**, *114*, 11560−11566.
(19) Choi, C. S.; Prince, E. *Acta Crystallogr.* **1972**, *B28*, 2857−2862.
(20) McCrone, W. C. *Anal. Chem.* **1950**, *22*, 954−955.
(21) Karpowicz, R. J.; Brill, T. B. *J. Phys. Chem.* **1984**, *88*, 348−352.
(22) Baer, B. J.; Oxley, J.; Nicol, M. *High Pressure Res.* **1990**, *2*, 99−108.
(23) Dreger, Z. A.; Gupta, Y. M. *J. Phys. Chem. B* **2007**, *111*, 3893−3903.
(24) Brill, T. B.; Sergio, T.; Karpowicz, R. *Ind. Eng. Chem. Prod. Res. Dev.* **1983**, *22*, 363−365.
(25) Torres, P.; Cotte, I.; Hernandez, S. P.; Mina, N.; Santana, A.; Chamberlain, R.; Lareau, R.; Castro, M. *J. Phys. Chem. B* **2004**, *108*, 8799−8805.
(26) An, Q.; Zybin, S. V.; Goddard, W. A., III; Jaramillo-Botero, A.; Blanco, M.; Luo, S. N. *Phys. Rev. B* **2011**, *84*, 220101.
(27) Cawkwell, M. J.; Ramos, K. J.; Hooks, D. E.; Sewell, T. D. *J. Appl. Phys.* **2010**, *107*, 063512.
(28) Plaskin, I.; Coffey, C. S.; Mendes, R.; Ribeiro, J.; Campos, J.; Direito, J. 13th Symposium International on Detonation, ONR 351-07-01, 2006; p 319.